POLITECNICO DI TORINO
Repository ISTITUZIONALE

Modelling friction at the mechanical interface between the human and the exoskeleton

(Article begins on next page)

08 November 2022

Modelling friction at the mechanical interface between the human and the exoskeleton

Divyaksh Subhash Chander* and Maria Pia Cavatorta

Department of Mechanical and Aerospace Engineering,
Politecnico di Torino,
Corso Duca Degli Abruzzi, 24
10129 Torino, Italy
Email: chander.divyaksh@polito.it
Email: maria.cavatorta@polito.it
*Corresponding author

Abstract:

In virtual assessments of exoskeletons, often, friction is not modelled even though the actual interface consists of straps or moulded surfaces, where friction could play a significant role. In this work, the human-exoskeleton interaction during the use of a passive lower limb exoskeleton is modelled in three test cases through two different interface models. In particular, a model introducing friction at the human-exoskeleton interface is compared with a more conventional model that uses a kinematic joint to simulate the interface forces. Both the models show a good match between the empirical and predicted distribution of body weight between the subject and the exoskeleton. However, the results also show different trends of the moment required at the assisted joint by the different interface models, highlighting the importance of a realistic interface model to investigate the effectiveness of the exoskeleton in virtual assessments.

Keywords:

Musculoskeletal model; industrial exoskeleton; virtual assessment; human-exoskeleton interaction; passive exoskeleton; interface forces; biomechanics; exoskeleton effectiveness; friction modelling; lower limb exoskeleton

Biographical Notes: Divyaksh Subhash Chander received his MSc in Automotive Engineering at the Politecnico di Torino, where he is currently pursuing his PhD. His research interests include biomechanical analysis of exoskeletons through musculoskeletal modelling.

Maria Pia Cavatorta is an Associate Professor at the Department of Mechanical and Aerospace Engineering at Politecnico di Torino, Italy. She received her MSc in Mechanical Engineering in 1995 and a PhD in Machine Design in 1999 at the same University. From 1997 to 1998, she was a visiting scholar at the University at Urbana-Champaign (USA). For the past decade, her research interests have been focused on the integration of human factors and biomechanics into workplace design.

1.0 Introduction

The underlying idea behind the development of exoskeletons is to support the user through passive or active assistance. The effects of the use of an exoskeleton on the human can be assessed in multiple ways. Experimental studies simulate pre-defined activities with and without the exoskeleton and measure objective (measures of performance and time, muscle activity through EMG, contact pressure, heart rate) and subjective (perceived exertion, discomfort, usability) responses (Alabdulkarim and Nussbaum, 2019; Amandels et al., 2019; Baltrusch et al., 2018; Huysamen et al., 2018; Spada et al., 2017). Some experimental studies are also supported by biomechanical models that are used to estimate changes in muscle activities or joint moment requirements (Koopman et al., 2019; Picchiotti et al., 2019; Spada et al., 2019; Weston et al., 2018). Another approach is the purely virtual assessment of exoskeletons. This is especially useful during the design and the redesign phase where various configurations of mechanisms and assistance are studied and optimized in a virtual environment (Agarwal et al., 2016; Fournier et al., 2018; Hansen et al., 2018; Jensen et al., 2018; Tröster et al., 2018; Zhou et al., 2017). Additionally, virtual modelling of exoskeletons also allows the study of the combined human-exoskeleton model in the digital factory (Constantinescu et al., 2016).

Virtual assessment through musculoskeletal models provides biomechanical outputs such as muscle activity, joint moments and reaction forces that are widely used to assess the effects of the use of an exoskeleton. In virtual modelling, often the contact interface between the human and the exoskeleton is defined as a kinematic joint between a point on the human model and a point on the exoskeleton. The definition of the joint is essential to study the kinematics of the combined human-exoskeleton model and it also provides an estimate of the reaction forces exchanged at the interface by solving the Newton-Euler equations for dynamic equilibrium in multibody systems (Agarwal et al., 2016; Gordon et al., 2018; Guan et al., 2016; Hansen et al., 2018; Harant et al., 2017; Jensen et al., 2018; Zhou et al., 2017). Another approach to estimating the interface forces is by adding force-generating elements to produce forces in the necessary degrees of freedom while maintaining the kinematic joint for the study of kinematics only. In this way, the interface forces could be estimated by considering these force generators under a global optimization problem to reduce the muscular effort (Fournier et al., 2018; Tröster et al., 2018). However, studying contact interface forces by these methods brings forward a major limitation as these methods do not simulate frictional forces. Without due consideration of frictional forces, high shear force components, unrelated to the normal force component, could be generated at the interface in the model. In reality, however, high shear forces would require high normal forces as the contact between the human and the exoskeleton is often through straps or surfaces that are moulded to the shape of the body. In the presence of straps or moulded contact surfaces, shear or frictional forces are bound to the normal forces and could play a significant role in the forces exchanged at the human-exoskeleton interface. While high normal forces could create discomfort at the interface due to the high contact pressure, on the other hand, an increased effort could be required from the user to compensate for the inadequate shear force as compared to the simulated shear force. Thus, there

is a need to use a more detailed contact model to simulate the contact forces at the human-exoskeleton interface in virtual assessments.

In a few studies, the human-exoskeleton interface forces have been simulated through a contact model that is capable of generating normal and shear contact forces. Cho et al., 2012 evaluated the effect of adding straps to an exoskeleton and found that the straps are especially useful to reduce body joint torques when handling heavy loads. Jung et al., 2017 developed a musculoskeletal model to study an ankle exoskeleton. However, both of these studies evaluated the exoskeletons virtually only. Spada et al., 2019 used a method similar to the ones used in (Cho et al., 2012; Jung et al., 2017) to study a lower limb passive exoskeleton. They found a good match between the simulated and empirical body weight distribution between the subject's feet and the exoskeleton. It confirmed the potential of using this method to estimate the human-exoskeleton interface forces that could be distributed over a surface and estimate shear forces at the contact.

The aim of this work is to study in detail the contact model between the human and the exoskeleton presented in (Spada et al., 2019). Further, the contact model will be compared with the simulation of the human-exoskeleton interface forces through the conventional method of using a kinematic joint between the human and the exoskeleton. The contact model presented in Spada et al., 2019 is based on an existing method to predict the ground reaction forces (GRF) and moments (Fluit et al., 2014; Skals et al., 2017). The exoskeleton chosen for the analysis, Chairless Chair® (noonee AG, Switzerland), offered a similar contact condition between the user's thigh and the seat of the exoskeleton in the seated condition to that of the contact between the foot and the ground as validated in the GRF prediction method. The seat presented a fixed surface on which the user sits and transfers a part of the body weight to the ground through the exoskeleton. The advantages and limitations of using the GRF prediction method to estimate the contact forces at the human-exoskeleton interface will be addressed in this work.

2.0 Materials and methods:

The aim of this work was to investigate the use of the GRF prediction method to estimate the exchange of forces at the human-exoskeleton interface. The typical simulation framework for the use of exoskeletons consists of the human model, the exoskeleton model, and the kinematic and dynamic interactions between the human and the exoskeleton model. All these components are then integrated to simulate some use cases of the exoskeleton and make the required analyses.

2.1 Exoskeleton and the use case:

The exoskeleton used in this work, the Chairless Chair, is a commercially available passive exoskeleton for the lower limbs. The exoskeleton allows the user to walk and work in a standing or a seated posture. It is intended for industrial use and aims to replace working with a bent trunk by working in a seated posture. In the standing configuration, the exoskeleton is loosely attached to the legs of the user and follows the user without contacting the ground while the user walks. Instead, as the user starts to sit, the exoskeleton rests on the ground and bends at its central revolute joint, which corresponds with the knee joint of the user, and stops at a user-selected angle. This enables the user to sit on the exoskeleton and distribute the body weight between his/her legs and the legs of the exoskeleton. The user can have a continuous adjustment of the seat height between a minimum height, defined as the low-seat configuration, and a maximum height, defined as the high-seat configuration.

As described in (Spada et al., 2019), the Chairless Chair was tested in the laboratory by 14 technical employees of both genders to verify if the distribution of the subject's weight between the subject and the exoskeleton remained within a given range, regardless of the subject's anthropometry and the sitting height of the exoskeleton. Three measurements per subject were taken for each of the three sitting heights: the low-seat configuration, the high-seat configuration, and a seat height selected by the subjects as the most comfortable, defined as the comfort-seat configuration. Results from these tests indicated that the body weight distribution between the subject and the exoskeleton was not significantly influenced by the anthropometry or the sitting height. Instead, training and user confidence appeared to be a requisite for the effective use of the exoskeleton.

Therefore, for the purpose of musculoskeletal modelling, weight distribution between the subject and the exoskeleton was measured through a scale in three different conditions with different arm and trunk postures to simulate working at elbow height, reaching an overhead point with the arms raised and lateral reaching to the right with both hands (Fig.1). These empirical trials were performed in the comfort-seat configuration by a single subject who had received adequate training in the use of the Chairless Chair (Spada et al., 2019).

Fig.1: The three test conditions: a.) Working at elbow height, b.) Reaching with arms raised, and c.) Lateral reaching (to the right). The red sphere is the centre of mass of the mannequin.

The percentage of body weight supported by the Chairless Chair is a key metric to measure the assistance provided by the exoskeleton while in use and is utilized in this work to define the effectiveness of the exoskeleton. The use of the exoskeleton in the three different conditions represented three different weight distributions between the user and the exoskeleton. These conditions served to test the model in three different scenarios, one of which also considered an asymmetric distribution of weight between the right and left side. Working at elbow height represented a stable condition where the user could easily maintain the balance and equilibrium between his/her and the exoskeleton's legs. This condition allowed the user to be optimally supported by the exoskeleton. Instead, reaching with arms raised and extended represented a more challenging condition that required the user to slightly lean forward and reach an overhead point, while lateral reaching to the right added an additional element of difficulty in terms of asymmetry. In such conditions, the user would be required to shift the balance between his/her and the exoskeleton legs and would be forced to support a greater percentage of the body weight by his/her own legs rather than the exoskeleton. The model was tested in these three conditions by simulating the static postures observed during the empirical trials. It must be emphasized here that the latter two reaching conditions are neither recommended by the manufacturer nor by the authors. Excessive leaning presents an increased risk of falling. The reaching conditions were tested to verify the capability of the musculoskeletal model to handle different conditions.

2.2 Musculoskeletal Modelling:

The musculoskeletal model was analysed using the software AnyBody Modeling Systems™ (AMS™) (AnyBody Technology A/S, Denmark) version 7.0.1. AMS uses a multibody dynamics approach to analyse the musculoskeletal systems of humans (Damsgaard et al., 2006). The developers of the software also maintain an open repository of musculoskeletal models and some application examples that could be readily used in AMS. The starting point of the simulation in this work was the Human Standing Template available in version 1.6.6 of the repository (Lund et al., 2017).

AMS uses inverse dynamics analysis to calculate internal muscle forces required to enable the musculoskeletal human model to perform known motions and exchange known forces with its surroundings. The redundancy problem that arises due to an excess of force-producing muscles in the human model than strictly necessary to perform a given task is resolved by framing the dynamic equilibrium equations as an optimization problem (Rasmussen et al., 2001). In this work, the optimization problem defines the objective function to be minimized as the polynomial criterion with power, $p = 3$:

$$G\left(\boldsymbol{f}^{(\boldsymbol{M})}\right) = \sum_{i=1}^{n^{(M)}} \left(\frac{f_i^{(M)}}{N_i}\right)^p \tag{1}$$

subject to the following constraints:

$$\boldsymbol{Cf} = \boldsymbol{r} \tag{2}$$

5

$$\left(f_i^{(M)}\right) \geq 0 \; ; \; i \in \left\{1, \ldots, n^{(M)}\right\} \tag{3}$$

where *G* is the objective function of the recruitment strategy stated in terms of the muscle forces, *f*$^{(M)}$. N_i is a measure of the muscle's strength at the current working conditions. $n^{(M)}$ is the number of muscles. ***C*** = *[**C**$^{(M)}$**C**$^{(R)}$]* is the coefficient matrix of the unknown forces vector, ***f*** = *[**f**$^{(M)T}$**f**$^{(R)T}$]^T*. Superscripts (M) and (R) designate terms related to muscle forces and joint reactions, respectively. Instead, ***r*** is a vector of the known external and inertial forces. The constraint (3) restricts the muscles to pulling only and prevents pushing.

2.2.1 Human Model

The human model of the Human Standing template was set up to use the 3-element muscle model, which is the most detailed muscle model available in the AMS and is based on a modified Hill muscle model (Zajac, 1989). Further, the human model was scaled to the height (165.0 cm) and the weight (73.8 kg) of the subject using the length-mass-fat scaling law (Rasmussen et al., 2005). These settings have also been used in past works (Chander and Cavatorta, 2018; Farahani et al., 2016). While subject-specific models could increase accuracy (Oomen et al., 2015), they require additional input data in the model, which was not feasible for the scope of this work.

The template was modified by removing the default constraint on the Centre of Mass (CoM) of the human model. This constraint forced the CoM of the model to be vertically aligned with the origin of the reference system and the midpoint of the line joining the right and left ankle to ensure standing balance. However, it also restricted the ability of the model to correctly simulate the seated posture with the Chairless Chair, which required the model to support its weight between its own legs and the exoskeleton.

2.2.2 Ground reaction force prediction

The existing contact between the human model and the ground was replaced by adopting a method to predict ground reaction forces and moments using only the kinematic data (Fluit et al., 2014). This method has also been adopted in other works (Eltoukhy et al., 2017; Peng et al., 2018; Skals et al., 2017). In this work, the method reported in (Skals et al., 2017) has been used. In this method, the GRF is predicted through unidirectional force-producing actuators that are added between the ground and the feet of the subject. Mathematically, the actuators are modelled like the skeletal muscles and are included in the muscle recruitment optimization problem during the inverse dynamics analysis to determine their activation level. Just like skeletal muscles, these muscle-like actuators generate force in one direction only and the value of force is obtained as the product of the activation level and the strength of the muscle. However, the strength of these actuators was much higher than the skeletal muscles in order to ensure a low activation cost in the optimization problem. At the bottom of each foot, 25 contact points were defined and at each of these points, five actuators were created. One actuator was aligned along the normal to the ground plane to generate force in the vertical direction. While the other four actuators were aligned in pairs along the anterior-posterior and the medial-lateral directions to generate the positive and negative static

friction forces. These four actuators were modelled in such a way that their actuation also resulted in the generation of a normal force, Fn, such that the friction force generated by the actuator is equal to µFn, where µ is the coefficient of friction. Therefore, the net vertical force at any contact point was the sum of the vertical forces produced by all the five actuators and the friction force was bound to the normal force by the coefficient of friction (Skals et al., 2017).

2.2.3 Exoskeleton model

A functional CAD (computer-aided design) model of the Chairless Chair was created in SolidWorks® 2012 (Dassault Systèmes SOLIDWORKS Corporation) software. The exoskeleton model was imported into AMS using the AnyExp4SOLIDWORKS™ (AnyBody Technology A/S, Denmark) plugin (version 1.1.0). The plugin was used to translate the CAD model into a script file that could be read by AMS. The translated script file maintains the mass, inertia, geometry, and joints as defined in the CAD environment. Nevertheless, once translated into a script file, these properties could be easily modified inside the AMS environment, independently from the CAD environment. As the central revolute joint of the Chairless Chair locked at the desired seating height, the central joint in the exoskeleton model was defined to produce all the reaction forces and moments necessary to maintain the orientation of the exoskeleton.

2.2.4 Human-exoskeleton model

The combined human-exoskeleton model consisted of defining the kinematic and dynamic interactions between the human model and the exoskeleton, and the ground and the exoskeleton. In this work, the kinematic interactions between the exoskeleton and the human model were not of significance as only static simulations during the use of the Chairless Chair were considered. The human model and the exoskeleton were positioned by replicating the corresponding postures/positions from the empirical trials. On the other hand, the dynamic interaction between the human model and the exoskeleton was the focus of this work. The aim of this work was also to compare the human-exoskeleton interface forces estimated by the GRF prediction method with those estimated by the conventional method of using a kinematic joint between the human and the exoskeleton. Thus, two models were set up to compare the human-exoskeleton interface forces estimated by the two different methods.

GRF prediction model (Model 1)

In Model 1, the dynamic interactions at the human-exoskeleton and the exoskeleton-ground interfaces were set up by adopting the same method as that used for predicting GRF. At the human-exoskeleton interface, the thigh of the human model was treated like the foot in the GRF prediction method, as described in section 2.2.2, and 21 contact points were created on each thigh. On the exoskeleton side, a contact detection zone was created on the exoskeleton seat. A planar contact detection zone was modelled to represent the seat surface. This surface was tangential to the seat at the central curve tracing the length of the seat. Thus, the normal to the planar surface was also normal to the seat surface at the central curve and the anterior-posterior axis was defined along the central curve of the seat. Instead, at the exoskeleton-ground interface, the exoskeleton leg was modelled like the human foot and 11 contact points were created at the base of each leg of the

7

exoskeleton. The ground was modelled in just the same way as the ground in the human-ground interface. In this way, the use of the method to predict GRF provided for an exchange of forces at both the human-exoskeleton and the exoskeleton-ground interfaces, thereby effectively creating a transmission of the body weight to the ground through the exoskeleton.

Overall, there were six implementations of the GRF prediction method in the model considering the right and left side separately for the three interfaces: human-ground, human-exoskeleton, and exoskeleton-ground. The method introduced coefficients of friction at every implementation, which is a potential advantage of this method compared to simulating the interface forces through a kinematic joint. However, setting the value of the coefficients could be challenging. Thus, a parametric study was performed to check the influence of the coefficient of friction at each interface on the model results and based on the results of this study, each of the coefficients of friction was set as 0.5 (section 3.1).

Kinematic joint model (Model 2)

A second human-exoskeleton model was set up wherein the human-exoskeleton interface was defined using a kinematic joint between a point on the human thigh and a point on the exoskeleton seat, on both the right and the left side, to compute the human-exoskeleton interface forces. All the six degrees of freedom of the kinematic joints were fixed at the interface. For the sake of comparison between the two methods, the point on the thigh corresponded with the central contact detection node and the point on the exoskeleton corresponded with the centre point of the contact detection zone. Further, the remaining two interfaces, that is, the exoskeleton-ground and the human-ground, were maintained the same as from the model with the GRF prediction method with the coefficients of friction as 0.5

2.3 Analysis and comparison of the two models:

After setting up the combined human-exoskeleton models, static postures were simulated to replicate the empirically observed postures during the three test conditions: working at elbow height, reaching with arms raised, and lateral reaching to the right. The same postures were used in both models. The net vertical force at both the feet was used as a measure of the weight supported by the legs of the human model in the simulations. As the weight of the subject was known, the weight of the subject supported by the exoskeleton was calculated as the difference between the subject weight and the weight supported by the legs of the subject. Additionally, measures of muscle activation and joint moments from both the models were noted as indicators of biomechanical requirements in the different test conditions. Muscle activation is defined as the ratio of the force produced by the muscle to its strength.

8

3.0 Results and Discussion

The aim of this work was to investigate the use of the GRF prediction method (Model 1) to estimate the interface forces between the human and the exoskeleton and to compare the results obtained from this model with those from the conventional model of using a kinematic joint at the interface (Model 2). The first part of this section focuses on the role of friction introduced by the GRF prediction method at the different interfaces in the model. The second part compares the results from Model 1 and Model 2. The section is concluded by the limitations of the method and future work.

3.1 Friction force at human-exoskeleton interface

Fig.2 depicts the percentage of the body weight supported by the exoskeleton, predicted by Model 1 as the coefficients of friction at each of the three interfaces (human-ground, human-exoskeleton, and exoskeleton-ground) are varied from 0.2 to 0.8 in steps of 0.025. The coefficients at the human-ground and exoskeleton-ground are considered equal and represented by the coefficient of friction at the ground. In this parametric study, the posture "working at elbow height" is used and remains the same across all the conditions. The figure shows the model sensitivity to the coefficient of friction at the human-exoskeleton interface. The percentage of body weight supported by the exoskeleton remains stable around 66% of the body weight for the coefficient values from 0.4 to 0.8. A change in the coefficient from 0.4 to 0.3 shows a sharp drop in the percentage of body weight supported by the exoskeleton. Meanwhile, for low values of the coefficient of friction at ground, a small transition zone can be observed where the percentage of body weight supported by the exoskeleton depends on both the coefficients of friction. Elsewhere, the model is resilient to changes in the coefficient of friction at the ground. The body weight acts in the vertical direction. As the exoskeleton seat presents an inclined surface, the friction force at the human-exoskeleton interface becomes important for the subject not to slip down along the seat. The model is able to capture this relevant detail, confirming the functionality of the static friction component in the model.

Fig.2: Parametric study of the coefficients of friction at the human-exoskeleton (Mu_SubExo) interface and the ground (Mu_Ground). Mu_Ground represents both the coefficients of friction at the exoskeleton-ground and the human-ground interfaces and considers them as equal.

Table 1 shows some of the biomechanical outputs at different values of the coefficient of friction at the human-exoskeleton interface. The loss of effectiveness of the exoskeleton for the coefficient values lower than 0.4 is also reflected in the significantly higher joint moment values at the knee. Supporting all the body weight on the legs requires more than 5 times the extension moment at the knee as compared to the case with optimal assistance from the exoskeleton. Meanwhile, at the ankle, the moment changes direction from a plantar flexion to a dorsiflexion moment. The change

9

to a dorsiflexion moment at the ankle indicates that the mannequin would lose its equilibrium as the centre of mass of the mannequin is behind the ankles. Consequently, the mannequin would not be able to maintain balance in the given posture without adequate support from the exoskeleton. Instead, the extension moment at the hip joint is required to maintain the posture of the upper half of the body and depends on the posture of the part of the body above the hips in the model. Unlike the knee and the ankle joints, the hip joint is above the human-exoskeleton interface and the load above the hip joint would not be affected by the distribution of body weight at the human-exoskeleton interface. The overall moment required at the hip joint would not be affected by the changes in the exoskeleton effectiveness as the posture remains unaffected. Loss of support from the exoskeleton would be balanced by the activation of muscles that span over the hip joint, such that the moment requirement at the hip is satisfied.

Table 1: Percentage of body weight supported by the exoskeleton and the joint moments at the hip, knee, and ankle joints for different values of the coefficient of friction (Mu) at the human-exoskeleton interface. The coefficients of friction at the other two interfaces are constant at 0.5 each. "-" sign indicates an opposite moment.

Thus, friction force is relevant at the human-exoskeleton interface, such that a reduction in the coefficient of friction significantly reduces the percentage of body weight supported by the exoskeleton, which consequently changes the biomechanical outputs from the model at the joints affected by the exoskeleton. Based on the results presented in Fig.2 and Table 1, all the three coefficients of friction were set as 0.5 for further analyses, such that the exoskeleton was able to offer adequate support.

3.2 Comparison of GRF prediction model (Model 1) and Kinematic joint model (Model 2)

The second aim of this work was to compare the results obtained from the GRF Prediction method with the results obtained from the conventional model of using a kinematic joint at the human-exoskeleton interface. Fig.3 plots the empirical and predicted percentage of body weight supported by the exoskeleton in the three test conditions. Both the models are able to capture the distribution of body weight between the subject and the exoskeleton in the different test conditions. The average error in the percentage of body weight supported by the exoskeleton in the elbow height and raised arms conditions is 10% for the model with the kinematic joint. The average error for the model with the GRF prediction method in the same conditions is only 1.5%. Instead, in the third condition of lateral reaching, the model with the kinematic joint predicts correctly the percentage weight supported by the exoskeleton, while the model with the GRF prediction method overestimates the support by 5%. When comparing the results of both the models, the model with kinematic joint estimates lower support by the exoskeleton as compared to the model with the GRF prediction method in all the three test conditions (Fig.3).

Fig.3: Percentage of body weight supported by the exoskeleton by the GRF prediction model, the kinematic joint model, and empirical values in the three test conditions.

10

Table 2 presents a comparison of the outputs from the two models. It compares the reaction forces at the human-exoskeleton interface, the muscle activation, and the joint moment requirements. The first two conditions, working at elbow height and reaching with raised arms, are symmetric and have equal values at the right and the left side. Instead, the values for both the right (R) and left (L) side are reported for lateral reaching.

Table 2: Comparison of the GRF prediction model (Model 1) and the kinematic joint model (Model 2). Reaction forces are expressed in the local reference system at the central point of contact where the X-axis is defined as normal to the seat surface (positive upwards) and the Y-axis is defined tangential to the seat surface and oriented along the length of the seat (positive upwards). The Z-axis is defined by the conventional Cartesian system.

It is clear from the results presented in Table 2 that there are certain differences between the two models. First and foremost, a difference in the interface forces can be observed between the two models. While the GRF prediction method simulates the frictional forces, the kinematic joint does not consider frictional forces and, thus, does not allow for evaluating how different interface properties could modify the effectiveness of the exoskeleton. Resolving the net reaction force from the kinematic joint model in the normal and shear direction shows that there is no consistency in the ratio of the shear force to normal force in the three test conditions. In the case of lateral reaching to the right, the reaction forces of the GRF prediction model show that almost no reaction force is exchanged at the left side, despite there being contact. This would also be the real situation as the subject reaches a distant point asymmetrically. One of the four supports would become unloaded and the body weight would be distributed between the remaining three supports.

In terms of biomechanical outputs, a major difference exists between the trends of the knee extension moment requirement from the two models. Fig.4 plots the knee extension moment from the two models in the three test conditions. In the case of lateral reaching, the right and the left knee extension moments are indicated in the graph with the trend line passing through the mean value of the right and the left knee extension moment. The GRF prediction method demonstrates a slight increase in the requirement of knee extension moment as the test condition becomes more challenging and the percentage of body weight supported by the exoskeleton decreases. In Model 1, the exoskeleton is able to isolate the knee joint from a significant increase in the loading despite the increased body weight supported by the subject. The effect of the exoskeleton on the knee moment requirement is also apparent in the case of lateral reaching to the right. The right knee extension moment is lower than the left knee extension moment despite a greater portion of the body weight supported by the right side (65%) as compared to the left side (35%), which is also evident from a higher hip extension moment at the right hip. On the right side, the exoskeleton effectively supports a substantial part of the body weight. Instead, on the left side, most of the body weight is supported by the left leg without any relief from the exoskeleton as is also confirmed by the negligible human-exoskeleton interface forces on the left side (Table 2).

On the other hand, the kinematic joint model not only estimates a lower knee extension moment than the GRF prediction method despite lesser support from the exoskeleton but also, and rather counter-intuitively, demonstrates a reduction in the knee extension moment in more challenging test conditions (Fig.4). The Chairless Chair offers fixed support, on which the user rests and it is unlikely that the exoskeleton would be able to reduce the knee extension moment requirement as it becomes less effective. In Model 2, the kinematic joint at the human-exoskeleton interface provides the additional forces and, crucially, higher moments to offload the knee joint in an unrealistic manner as the posture becomes more critical.

Fig.4: Knee extension moments by the GRF Prediction model and the kinematic joint model in the three test conditions. In the case of lateral reaching, the trend line passes through the mean of the right and the left knee extension moment.

At the ankle joint, the kinematic joint model again estimates a lower plantar flexion moment requirement as compared to the GRF prediction method. Nonetheless, the ankle plantar flexion moment from both the models increases as the posture becomes more challenging. Instead, the moment requirement at joints above the human-exoskeleton interface, such as the hip, trunk, and shoulder are not affected by the presence of the exoskeleton, as also discussed in section 3.1, and demonstrate similar biomechanical outputs from both the models. These joints support the same weight that is dependent on the posture. Virtually no differences can be observed in the muscle activations in the upper limbs, trunk and the lower limbs and the hip extension moment (Table 2).

To conclude, it appears from the results of the knee extension moment that changing the contact model between the human and the exoskeleton can change the results of the biomechanical analysis. As seen in this work, changing the contact model resulted in the exchange of different interface forces. Different interface forces would consequently require different muscle forces to balance the external forces. However, it is critical to note that the different contact models could also result in different trends of key biomechanical outputs that are directly affected by the assistance from the exoskeleton, such as the knee extension moment in this work. This could be especially relevant in purely virtual assessments of exoskeletons as these evaluations are based on biomechanical outputs (Agarwal et al., 2016; Jensen et al., 2018; Zhou et al., 2017). The authors are not aware of past studies comparing different contact models between the human and the exoskeleton. However, Agarwal et al., 2016 and Fournier et al., 2018 suggest that a detailed human-exoskeleton interaction model could improve the analyses. Further studies on a comparison of contact models at the human-exoskeleton interface in different exoskeletons are needed.

3.3 Limitation and Future work

Firstly, as mentioned in section 2.2.4, a planar contact detection zone was used to model the seat. However, the planar contact detection zone can approximate only a small area of the seat that could be considered having a planar area. The actual seat presents a curved profile to the human leg, providing a continuously varying angle at the interface. It is highly probable that the interface

12

forces would be exchanged at different orientations and in different proportions in different zones of the seat. The study of the coefficients of friction at the different interfaces showed that the coefficient of friction is especially relevant at inclined surfaces. Thus, the planar contact detection zone limits the area of the seat that can be considered as an accurate representation of the seat in the model with respect to the inclination of the seat.

The limitation of the planar contact detection zone to model a restricted area of the seat could be particularly significant in the simulation of the high-seat configuration that presents the exoskeleton seat at a greater inclination. In the high-seat configuration, the contribution from the more horizontally oriented part of the seat could be significant for the effectiveness of the exoskeleton. Thus, another study was performed to see the influence of the inclination of the seat on the predicted percentage of body weight supported by the exoskeleton. In this parametric study (Fig.5), the percentage of the body weight supported by the exoskeleton as predicted by GRF prediction model is reported as a function of the angle of the contact detection zone and the coefficient of friction at the human-exoskeleton interface in the high-seat configuration. The angle of the contact detection zone was varied between 0 and 28° in steps of 1° to represent the varying orientation at which the curved exoskeleton seat could support the user, while, the coefficient of friction at the human-exoskeleton interface was varied from 0.2 to 0.8 in steps of 0.025.

Fig.5: Parametric study of the coefficient of friction at the human-exoskeleton interface (Mu_SubExo) and the angle of the exoskeleton seat (Angle_SubExo). Angle_SubExo = 0° represents the orientation of the seat in the high-seat configuration. The angle is increased in steps of 1° until 28° to represent a more horizontal orientation

The second parametric study provides additional confirmation of the effectiveness of the static friction component in the model. In this study, an interaction between the angle of the contact detection zone and the coefficient of friction at the human-exoskeleton interface can be observed (Fig.5). A more vertical orientation of the seat (as indicated by a lower value of contact angle) requires a higher coefficient of static friction for the exoskeleton to effectively support the body weight.

In the high-seat configuration, the exoskeleton is able to support only 58% of the body weight in the optimal conditions compared to 66% of the body weight in the comfort-seat configuration while working at elbow height. The high-seat configuration presents a more vertically oriented seat that would lead to an increased tendency of slip, thus limiting the weight that could be supported by the exoskeleton unless compensated by an increased coefficient of friction. Indeed, the increased slip in the high-seat configuration was also confirmed by the subjects (Luger et al., 2019; Spada et al., 2019). The ability of the model to consider the coefficient of friction, along with the angle of contact of the exoskeleton, could be relevant to select appropriate textiles for the seat fabric and the clothing of the user.

The results of the parametric study between the angle of the contact detection zone and the coefficient of friction at the human-exoskeleton interface confirm the importance of the angle of

13

the contact detection zone, besides the coefficient of friction, for effective transfer of the body weight by the exoskeleton. Therefore, a planar contact detection zone cannot be used to model a seat with significant curvature. For the future, the authors are considering substituting the single planar contact detection zone containing 21 contact nodes with multiple planar contact detection zones, each with a single contact node. This could be a way to address the problem as the multiple contact detection zones could be distributed along the seat surface with each zone being tangential to the corresponding seat surface.

Secondly, the Chairless Chair includes an elastic strap that runs around the thigh to maintain the position of the seat relative to the leg of the subject especially during walking. This strap is a part of the human-exoskeleton interface and would have contributed towards the forces exchanged between the human and the exoskeleton seat. This strap was not modelled as the contribution of the strap is minor compared to the forces exchanged between the human and the seat in the seated posture. Nonetheless, while the kinematic joint model rigidly fixes the exoskeleton to the human mannequin and provides reaction forces in all the directions, the GRF prediction model has only one unidirectional force actuator in the vertical direction and is unable to model the force of the strap to prevent the separation of the seat and the leg. Modelling the strap could have affected the comparison between the results of the GRF prediction model and the kinematic joint model slightly, especially in the lateral reaching posture with its trunk twisting.

4.0 Conclusion

Virtual assessment of exoskeletons can be useful to optimize the design of an exoskeleton by studying the interaction between the human and the exoskeleton. Accurate modelling is a prerequisite for virtual assessment to be reliable and useful. Conventionally, the interface between the human and the exoskeleton is modelled as a kinematic joint between a point on the human and a point on the exoskeleton rather than a contact between the human and straps or moulded surfaces as is often the case in reality. The kinematic joint, while essential to study the kinematics of the combined human-exoskeleton system, is unable to consider the frictional forces due to the straps in its estimate of the human-exoskeleton interface forces. In this work, a method to predict GRF was used to model the contact between the human and the seat of a lower limb passive exoskeleton and the method's estimate of the human-exoskeleton interface forces was investigated. The GRF prediction method is able to consider the frictional forces at the interface. Additionally, the human-exoskeleton interface forces were also modelled using the conventional method of defining a kinematic joint at the interface and the results of both the models were compared.

The results showed that both the models can provide a good approximation of the percentage of body weight supported by the exoskeleton. However, this work demonstrated that there is a difference in the estimate of the interface forces by the two methods. Crucially, the difference in the interface forces by the two methods also changes the biomechanical outputs. In this work, a reversal in trend was observed in the joint moment requirement at the joint directly affected by the exoskeleton. Different trends of the key biomechanical outputs can be especially relevant during the design or redesign phase, where the exoskeleton could be optimized based on these biomechanical outputs.

The results, however, also point to a potential limitation of the method in modelling a curved surface by a planar surface. This limitation could be the subject of future studies wherein the curved surface could be modelled by multiple instances of planar contact detection zones, each of which could be oriented tangentially to the surface.

References:

Agarwal, P., Neptune, R. R., & Deshpande, A. D. (2016). A Simulation Framework for Virtual Prototyping of Robotic Exoskeletons. *Journal of Biomechanical Engineering*, *138*(6), 061004. https://doi.org/10.1115/1.4033177

Alabdulkarim, S., & Nussbaum, M. A. (2019). Influences of different exoskeleton designs and tool mass on physical demands and performance in a simulated overhead drilling task. *Applied Ergonomics*, *74*(August 2018), 55–66. https://doi.org/10.1016/j.apergo.2018.08.004

Amandels, S., Eyndt, H. O. het, Daenen, L., & Hermans, V. (2019). Introduction and Testing of a Passive Exoskeleton in an Industrial Working Environment. In S. Bagnara, R. Tartaglia, S. Albolino, T. Alexander, & Y. Fujita (Eds.), *Proceedings of the 20th Congress of the International Ergonomics Association (IEA 2018)* (pp. 387–392). Cham: Springer International Publishing.

Baltrusch, S. J., van Dieën, J. H., van Bennekom, C. A. M., & Houdijk, H. (2018). The effect of a passive trunk exoskeleton on functional performance in healthy individuals. *Applied Ergonomics*, *72*(July 2017), 94–106. https://doi.org/10.1016/j.apergo.2018.04.007

Chander, D. S., & Cavatorta, M. P. (2018). Multi-directional one-handed strength assessments using AnyBody Modeling Systems. *Applied Ergonomics*. https://doi.org/10.1016/j.apergo.2017.09.015

Cho, K., Kim, Y., Yi, D., Jung, M., & Lee, K. (2012). Analysis and Evaluation of a Combined Human-Exoskeleton Model Under Two Different Constraints Condition. *International Summit on Human Simulation (ISHS), St. Pete Beach, FL, May*, 23–25.

Constantinescu, C., Muresan, P. C., & Simon, G. M. (2016). JackEx: The New Digital Manufacturing Resource for Optimization of Exoskeleton-based Factory Environments. *Procedia CIRP*, *50*, 508–511. https://doi.org/10.1016/j.procir.2016.05.048

Damsgaard, M., Rasmussen, J., Christensen, S. T., Surma, E., & de Zee, M. (2006). Analysis of musculoskeletal systems in the AnyBody Modeling System. *Simulation Modelling Practice and Theory*, *14*(8), 1100–1111. https://doi.org/10.1016/j.simpat.2006.09.001

Eltoukhy, M., Kuenze, C., Andersen, M. S., Oh, J., & Signorile, J. (2017). Prediction of ground reaction forces for Parkinson's disease patients using a kinect-driven musculoskeletal gait analysis model. *Medical Engineering and Physics*, *50*, 75–82. https://doi.org/10.1016/j.medengphy.2017.10.004

Farahani, S. D., Svinin, M., Andersen, M. S., de Zee, M., & Rasmussen, J. (2016). Prediction of closed-chain human arm dynamics in a crank-rotation task. *Journal of Biomechanics*,

49(13), 2684–2693. https://doi.org/10.1016/j.jbiomech.2016.05.034

Fluit, R., Andersen, M. S., Kolk, S., Verdonschot, N., & Koopman, H. F. J. M. (2014). Prediction of ground reaction forces and moments during various activities of daily living. *Journal of Biomechanics*, *47*(10), 2321–2329. https://doi.org/10.1016/j.jbiomech.2014.04.030

Fournier, B. N., Lemaire, E. D., Smith, A. J. J., & Doumit, M. (2018). Modeling and Simulation of a Lower Extremity Powered Exoskeleton. *IEEE Transactions on Neural Systems and Rehabilitation Engineering*, *26*(8), 1596–1603. https://doi.org/10.1109/TNSRE.2018.2854605

Gordon, D. F. N., Henderson, G., & Vijayakumar, S. (2018). Effectively Quantifying the Performance of Lower-Limb Exoskeletons Over a Range of Walking Conditions. *Frontiers in Robotics and AI*, *5*(June). https://doi.org/10.3389/frobt.2018.00061

Guan, X., Ji, L., Wang, R., & Huang, W. (2016). *Optimization of an Unpowered Energy-stored Exoskeleton for Patients with Spinal Cord Injury*. 5030–5033. https://doi.org/10.1109/EMBC.2016.7591857

Hansen, C., Gosselin, F., Mansour, K. Ben, Devos, P., & Marin, F. (2018). Design-validation of a hand exoskeleton using musculoskeletal modeling. *Applied Ergonomics*, *68*, 283–288. https://doi.org/https://doi.org/10.1016/j.apergo.2017.11.015

Harant, M., Sreenivasa, M., Millard, M., Sarabon, N., & Mombaur, K. (2017). Parameter optimization for passive spinal exoskeletons based on experimental data and optimal control. *IEEE-RAS International Conference on Humanoid Robots*, 535–540. https://doi.org/10.1109/HUMANOIDS.2017.8246924

Huysamen, K., de Looze, M., Bosch, T., Ortiz, J., Toxiri, S., & O'Sullivan, L. W. (2018). Assessment of an active industrial exoskeleton to aid dynamic lifting and lowering manual handling tasks. *Applied Ergonomics*, *68*(April 2017), 125–131. https://doi.org/10.1016/j.apergo.2017.11.004

Jensen, E. F., Raunsbæk, J., Lund, J. N., Rahman, T., Rasmussen, J., & Castro, M. N. (2018). Development and simulation of a passive upper extremity orthosis for amyoplasia. *Journal of Rehabilitation and Assistive Technologies Engineering*, *5*, 205566831876152. https://doi.org/10.1177/2055668318761525

Jung, M., Fau, G., Letier, P., Mittag, U., Zange, J., Rittweger, J., & Runge, A. (2017). Musculoskeletal Simulation of SOLEUS Ankle Exoskeleton for Countermeasure Exercise in Space. In J. González-Vargas, J. Ibáñez, J. L. Contreras-Vidal, H. van der Kooij, & J. L. Pons (Eds.), *Wearable Robotics: Challenges and Trends* (pp. 391–396). Cham: Springer International Publishing.

17

Koopman, A. S., Kingma, I., Faber, G. S., de Looze, M. P., & van Dieën, J. H. (2019). Effects of a passive exoskeleton on the mechanical loading of the low back in static holding tasks. *Journal of Biomechanics*, *83*, 97–103. https://doi.org/10.1016/j.jbiomech.2018.11.033

Luger, T., Cobb, T. J., Seibt, R., Rieger, M. A., & Steinhilber, B. (2019). Subjective Evaluation of a Passive Lower-Limb Industrial Exoskeleton Used During simulated Assembly. *IISE Transactions on Occupational Ergonomics and Human Factors*, *0*(0), 1–10. https://doi.org/10.1080/24725838.2018.1560376

Lund, M. E., Damsgaard, M., Tørholm, S., Galibarov, P. E., & Jung, M. (2017). *The AnyBody Managed Model Repository (AMMR) (Version 1.6.6)*. https://doi.org/10.5281/ZENODO.1250765

Oomen, P., Annegarn, J., Rasmussen, J., Rausch, J., Siebertz, K., Verdijk, L., … Meijer, K. (2015). Development and validation of a rule-based strength scaling method for musculoskeletal modelling. *International Journal of Human Factors Modelling and Simulation*, *5*(1), 19–32. https://doi.org/10.1504/IJHFMS.2015.068121

Peng, Y., Zhang, Z., Gao, Y., Chen, Z., Xin, H., Zhang, Q., … Jin, Z. (2018). Concurrent prediction of ground reaction forces and moments and tibiofemoral contact forces during walking using musculoskeletal modelling. *Medical Engineering and Physics*, *52*, 31–40. https://doi.org/10.1016/j.medengphy.2017.11.008

Picchiotti, M. T., Weston, E. B., Knapik, G. G., Dufour, J. S., & Marras, W. S. (2019). Impact of two postural assist exoskeletons on biomechanical loading of the lumbar spine. *Applied Ergonomics*, *75*(September 2018), 1–7. https://doi.org/10.1016/j.apergo.2018.09.006

Rasmussen, J., Damsgaard, M., & Voigt, M. (2001). Muscle recruitment by the min/max criterion - A comparative numerical study. *Journal of Biomechanics*, *34*(3), 409–415. https://doi.org/10.1016/S0021-9290(00)00191-3

Rasmussen, J., De Zee, M., Damsgaard, M., Christensen, S. T., Marek, C., & Siebertz, K. (2005). A general method for scaling musculo-skeletal models. Paper presented at the *International Symposium on Computer Simulation in Biomechanics*, *2005,* Ohio, USA. https://vbn.aau.dk/ws/portalfiles/portal/72203766/ScalingAbstract.pdf (accessed 05 November 2019).

Skals, S., Jung, M. K., Damsgaard, M., & Andersen, M. S. (2017). Prediction of ground reaction forces and moments during sports-related movements. *Multibody System Dynamics*, *39*(3), 175–195. https://doi.org/10.1007/s11044-016-9537-4

Spada, S., Ghibaudo, L., Carnazzo, C., Di Pardo, M., Chander, D. S., Gastaldi, L., & Cavatorta, M. P. (2019). Physical and Virtual Assessment of a Passive Exoskeleton. *Advances in Intelligent Systems and Computing*. https://doi.org/10.1007/978-3-319-96068-5_28

Spada, S., Ghibaudo, L., Gilotta, S., Gastaldi, L., & Cavatorta, M. P. (2017). Investigation into the applicability of a passive upper-limb exoskeleton in automotive industry. *Procedia Manufacturing*, *11*(June), 1255–1262. https://doi.org/10.1016/j.promfg.2017.07.252

Tröster, M., Schneider, U., Bauernhansl, T., Rasmussen, J., & Andersen, M. S. (2018). Simulation Framework for Active Upper Limb Exoskeleton Design Optimization Based on Musculoskeletal Modeling. *Technische Unterstützungssysteme, die die Menschen wirklich wollen*, 345–353. https://vbn.aau.dk/ws/portalfiles/portal/292649860/M.Tr_ster_SmartASSIST_2018_021120 18_Paper_32.pdf (accessed 05 November 2019).

Weston, E. B., Alizadeh, M., Knapik, G. G., Wang, X., & Marras, W. S. (2018). Biomechanical evaluation of exoskeleton use on loading of the lumbar spine. *Applied Ergonomics*, *68*(July 2017), 101–108. https://doi.org/10.1016/j.apergo.2017.11.006

Zajac, F. E. (1989). Muscle and tendon: Properties, models, scaling, and application to biomechanics and motor control. *Critical Reviews in Biomedical Engineering*, *17*(4), 359–411.

Zhou, L., Li, Y., & Bai, S. (2017). A human-centered design optimization approach for robotic exoskeletons through biomechanical simulation. *Robotics and Autonomous Systems*, *91*, 337–347. https://doi.org/10.1016/j.robot.2016.12.012
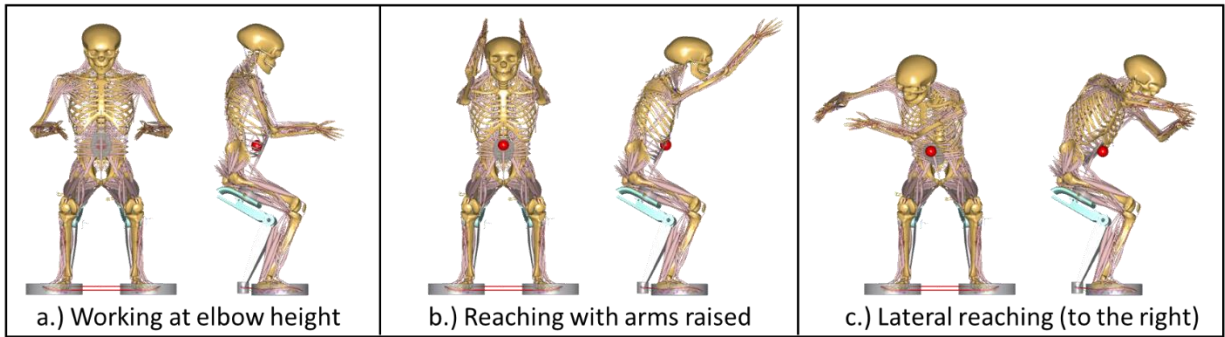
Figures:

Fig.1: The three test conditions: a.) Working at elbow height, b.) Reaching with arms raised, and c.) Lateral reaching (to the right). The red sphere is the centre of mass of the mannequin.
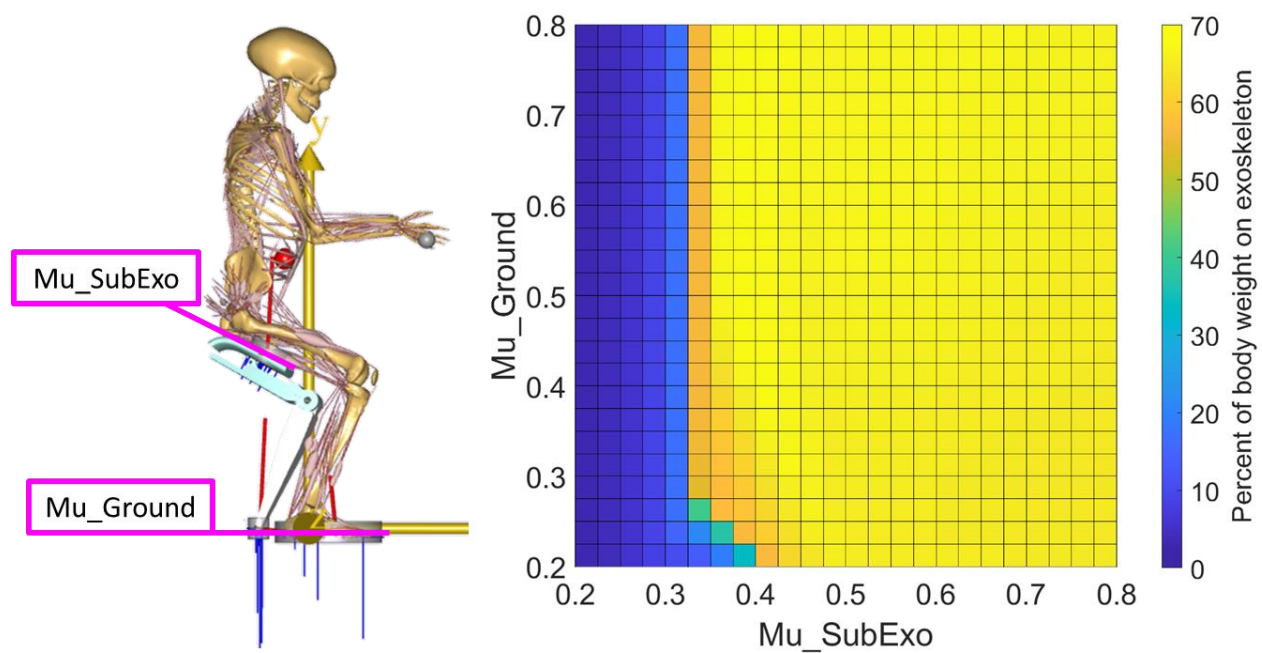
Fig.2: Parametric study of the coefficients of friction at the human-exoskeleton (Mu_SubExo) interface and the ground (Mu_Ground). Mu_Ground represents both the coefficients of friction at the exoskeleton-ground and the human-ground interfaces and considers them as equal.
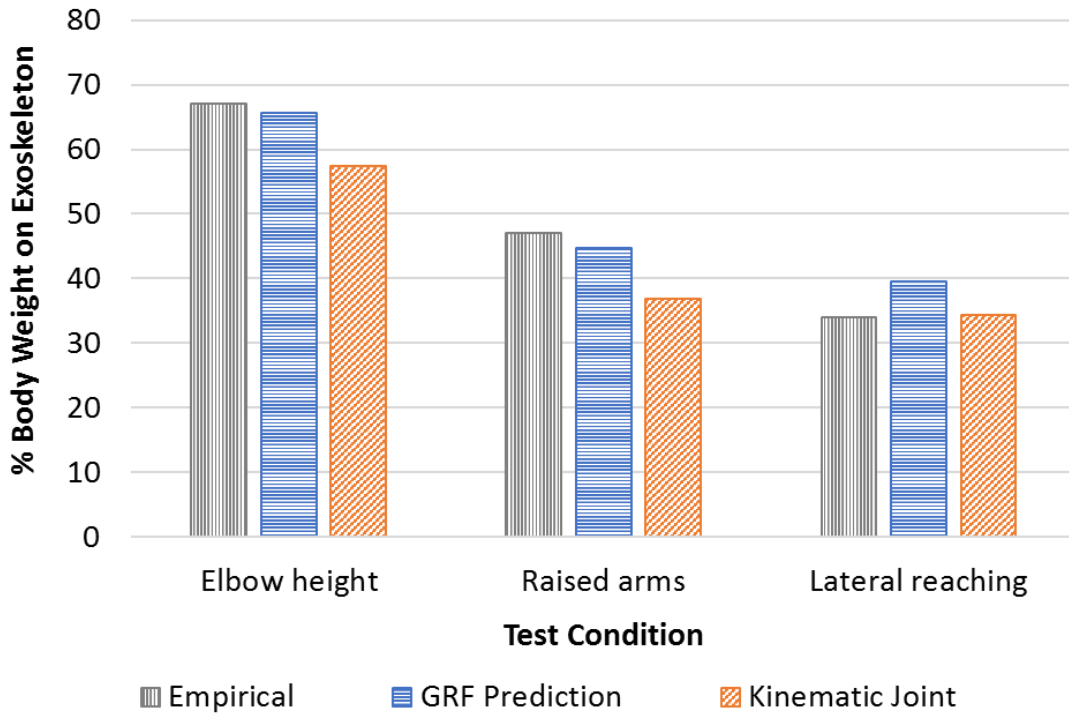
Fig.3: Percentage of body weight supported by the exoskeleton by the GRF prediction model, the kinematic joint model, and empirical values in the three test conditions.
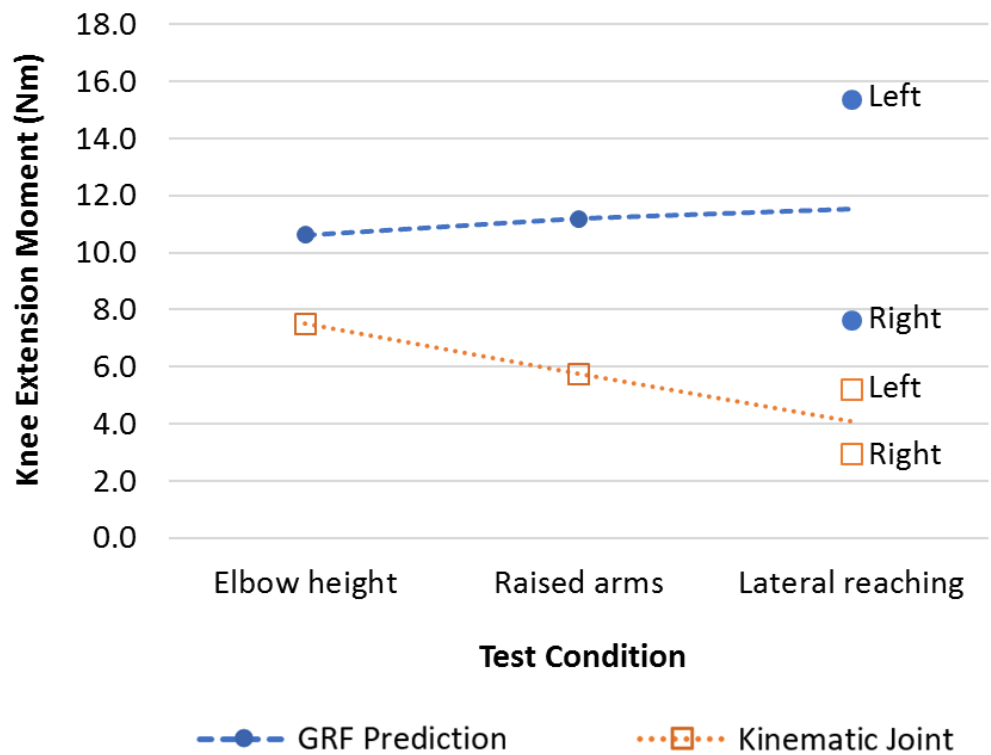
Fig.4: Knee extension moments by the GRF Prediction model and the kinematic joint model in the three test conditions. In the case of lateral reaching, the trend line passes through the mean of the right and the left knee extension moment.
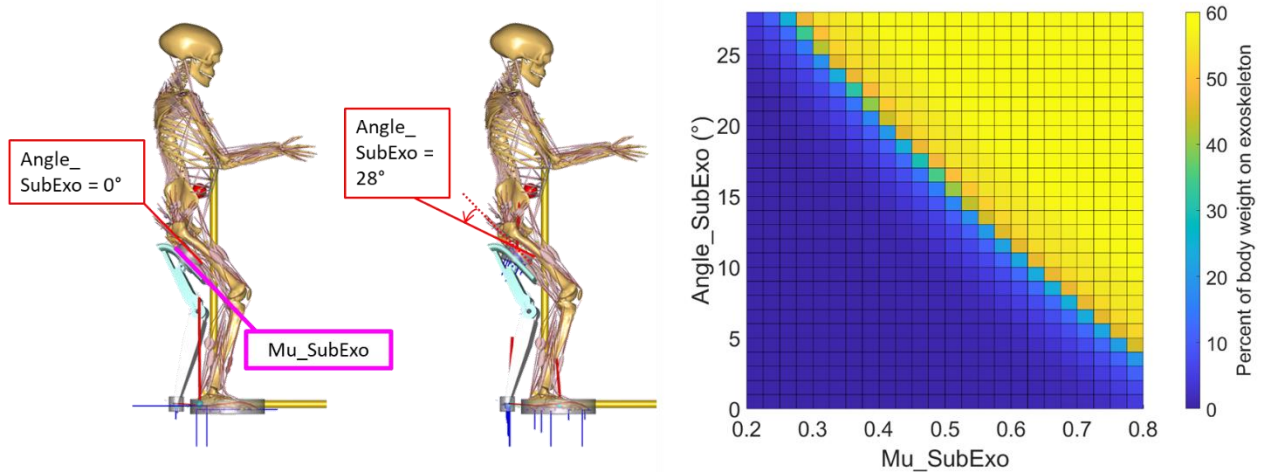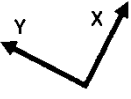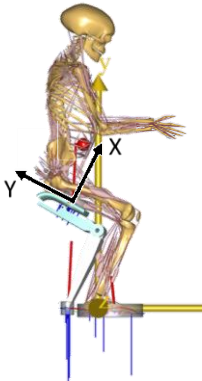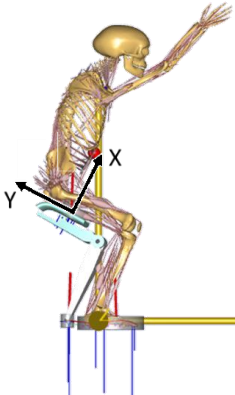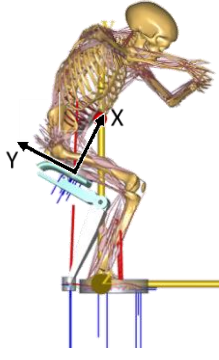
Fig.5: Parametric study of the coefficient of friction at the human-exoskeleton interface (Mu_SubExo) and the angle of the exoskeleton seat (Angle_SubExo). Angle_SubExo = 0° represents the orientation of the seat in the high-seat configuration. The angle is increased in steps of 1° until 28° to represent a more horizontal orientation.

Tables:

Table 1: Percentage of body weight supported by the exoskeleton and the joint moments at the hip, knee, and ankle joints for different values of the coefficient of friction (Mu) at the human-exoskeleton interface. The coefficients of friction at the other two interfaces are constant at 0.5 each. "-" sign indicates an opposite moment.

Mu at human-exoskeleton	0.6	0.5	0.4	0.3	0.2
% body weight on exoskeleton	66 %	66 %	66 %	17 %	3 %
Hip extension moment (Nm)	20.3	20.3	20.3	20.3	20.3
Knee extension moment (Nm)	10.3	10.6	13.9	53.5	55.4
Ankle plantar flexion moment (Nm)	9.0	9.0	11.1	-7.3	-11.9

Table 2: Comparison of the GRF prediction model (Model 1) and the kinematic joint model (Model 2). Reaction forces are expressed in the local reference system at the central point of contact where the X-axis is defined as normal to the seat surface (positive upwards) and the Y-axis is defined tangential to the seat surface and oriented along the length of the seat (positive upwards). The Z-axis is defined by the conventional Cartesian system.

Test condition	Working at elbow height		Reaching with raised arms		Lateral reaching (to the right)			
Local Reference System								
Model	Model 1	Model 2	Model 1	Model 2	Model 1		Model 2	
Estimated reaction forces at the human-exoskeleton interface (percentage of body weight in the local reference system)								
Fx	30 %	25 %	20 %	15 %	R: 34 %	L: 2 %	R: 23 %	L: 7 %
Fy	14 %	17 %	10 %	13 %	R: 17 %	L: 1 %	R: 18 %	L: 4 %
Fz	0 %	8 %	0 %	5 %	R: 0 %	L: 0 %	R: 7 %	L: 4 %
Muscle Activation (percentage)								
Trunk	23 %	23 %	40 %	40 %	100 %		100 %	
Upper Limbs	17 %	17 %	45 %	45 %	R: 99 %	L: 79 %	R: 99 %	L: 79 %
Lower Limbs	4 %	4 %	12 %	12 %	R: 18 %	L: 14 %	R: 18 %	L: 14 %
Joint Moments (Nm)								
Hip extension	20.4	20.4	38.1	38.1	R: 48.3	L: 37.4	R: 48.1	L: 37.6
Knee extension	10.6	7.5	11.2	5.8	R: 7.6	L: 15.4	R: 3.0	L: 5.2
Ankle plantar flexion	9.0	7.1	16.6	13.8	R: 18.7	L: 29.9	R: 15.4	L: 17.4